Arch. Mech., **58**, 4–5, pp. 459–475, Warszawa 2006

# Structure-controlled bifurcation in mathematical modelling of fibre spinning

A. ZIABICKI, L. JARECKI

*Institute of Fundamental Technological Research*
*Polish Academy of Sciences*
*Świętokrzyska 21, 00-049 Warsaw, Poland*
*e-mail:* aziab@ippt.gov.pl
*e-mail:* ljarecki@ippt.gov.pl

*In Memory of Professor Henryk Zorski*

In the mathematical model of melt spinning of fibres from crystallizing polymers the set of *conservation equations* is completed with structure-controlled *constitutive equations* and *structure evolution equations* describing kinetics of stress-induced crystallization. In a definite range of conditions, *bifurcation* of solutions is observed. Maximum filament velocity is limited and the same boundary conditions yield different steady-state dynamic and structure profiles. Bifurcation is observed when stress-induced crystallization leads to rapid solidification of the material. Critical conditions for bifurcation in melt spinning are analyzed and physical mechanism of such a behaviour is discussed.

## 1. Introduction

Computer modelling became a standard technique in polymer technology. Complexity of polymer behaviour including structure-dependent physical properties requires thorough adjustment of information to be input into governing equations. A model is as good (as bad) as the input information about the material behaviour.

In the course of simulation melt spinning of polyethylene terephthalate (PET), *bifurcation of steady-state solutions* was observed [1–3]. The same boundary conditions corresponded to two or more stress profiles and different structures of the resulting fibres. Multi-valued solutions appeared when polymer was crystallized under stress. Bifurcation of solutions may be important for the design and optimisation of industrial processes and determines the range of conditions under which stable formation of fibres is possible. In this paper we will analyse the physical source and mechanism of this phenomenon.

## 2. Description of the process

Figure 1 presents a scheme of single-filament, steady-state melt-spinning. Polymer melt is extruded at constant temperature, $T_0$, through a die of radius, $R_0$, at constant mass flow rate $W$, which determines constant extrusion velocity $V_0$. Fluid polymer jet is subjected to elongation in the direction $z$, and cooling by air with constant temperature $T_\infty \ll T_0$. At the distance $L$ from the extrusion point, solidified filament is collected with constant take-up velocity $V_L$.

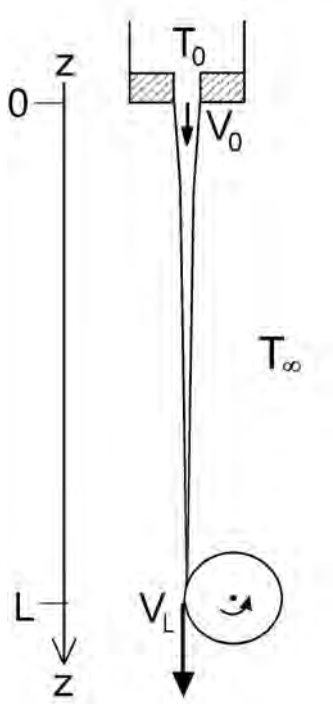


Fig. 1. Scheme of melt spinning.

## 3. Numerical simulation of melt spinning

Our simulations of polyethylene terephthalate spinning [1–4] were based on *thin filament approximation* neglecting radial distribution of kinematic and dynamic characteristics (velocity, $V$, temperature, $T$, axial tension, $F$) and replacing them with those *averaged* over the filament cross-section. This reduces the problem to one dimension – the coordinate $z$ – measured along the filament

from the extrusion point (spinneret), $z = 0$, to take-up point, $z = L$. The dynamic model involves structure-controlled rheological behaviour and evolution of polymer structure. It has been observed [1–3] that some solutions indicate bifurcation. Take-up velocity, $V_L$, plotted vs. initial tension, $F_0$, exhibits a maximum (Figs. 2 and 3). The same boundary condition $V(z = L) = V_L$ corresponds to different tensions and different filament structures. To elucidate the source and mechanism of this phenomenon we will analyse a simplified model, as compared to our early simulations.

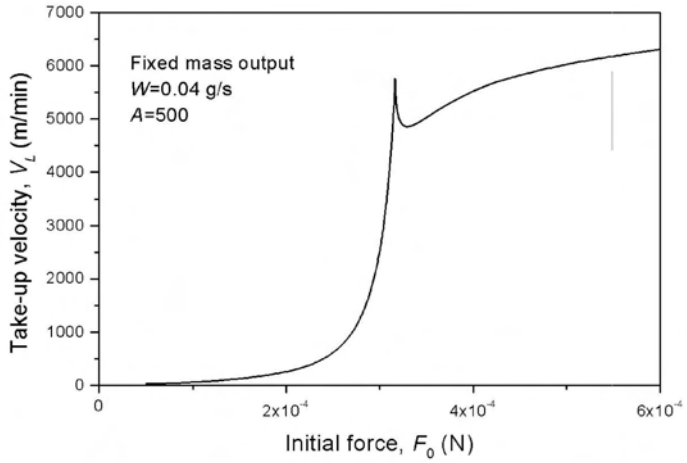


FIG. 2. The velocity-tension relation at constant mass output, $W = \text{const}$.

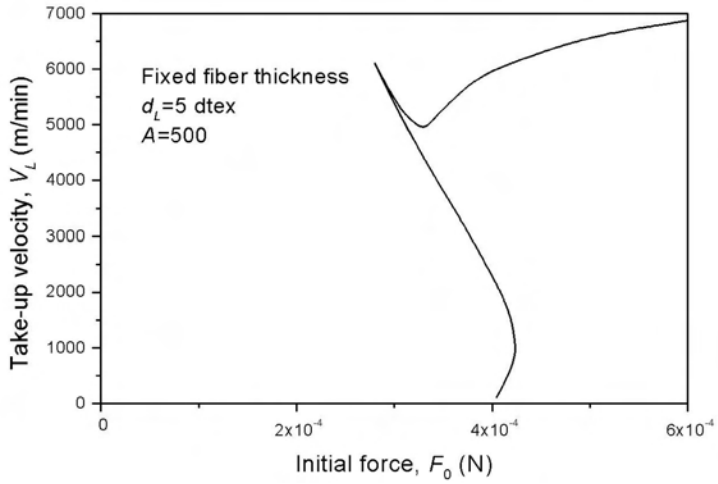


FIG. 3. The velocity-tension relation at constant filament thickness, $W/V_L = \text{const}$.

## 4. Simplified governing equations

Like in the earlier research [1–4], the steady-state, one-dimensional model based on thin-filament approximation will be analysed. The steady-state *mass conservation* equation assumes the form

$$\rho(z)\ \pi\ R^2(z)V(z) = \text{const} = W, \tag{4.1}$$

where $W$ is mass flow intensity, $\rho$ – density, $R$ – radius of the filament at the distance $z$ from the extrusion point, and $V$ – axial velocity averaged over the filament cross-section.

In the *equation of motion*, effects of gravity, surface tension and air drag are neglected, leaving only the convective inertial term

$$\rho V\frac{dV}{dz} = \frac{1}{\pi R^2}\frac{dF}{dz}, \tag{4.2}$$

where $F(z)$ is local tension at the distance $z$ from the extrusion point.

In the *energy conservation* equation, heat of crystallization and viscous dissipation are neglected leaving convective heat transfer from the surface of the filament to the cooling medium. The axial temperature gradient reduces to

$$\frac{dT}{dz} = -\frac{2\alpha^*}{\rho C_p RV}(T - T_\infty) = -\frac{2\pi R\alpha^*}{C_p W}(T - T_\infty), \tag{4.3}$$

where $C_p$ denotes specific heat of the filament, $\alpha^*$ – surface coefficient of heat transfer, and $T_\infty$ – constant temperature of the cooling medium. From Ref. [5]

$$\begin{aligned} Nu &= 0.42Re^{1/3}, \\ R\alpha^* &= 0.42\ \lambda_s\left(\frac{4WV}{\nu_s^2\rho\pi}\right)^{1/6} = \text{const}\ W^{1/6}V^{1/6}, \end{aligned} \tag{4.4}$$

where $\lambda_s$ and $\nu_s$ denote, respectively, thermal conductivity and kinematic viscosity of the cooling medium (air). Equations (4.3) and (4.4) reduce to

$$\frac{dT}{dz} = -\text{const}\, W^{-5/6}V^{1/6}(T - T_\infty). \tag{4.5}$$

The conservation equations are completed with structure-controlled *constitutive* equation and *structure evolution* equation.

The simplest constitutive model is used – incompressible Newtonian fluid with position-dependent viscosity, $\eta(z)$. Stress tensor, $\mathbf{p}$, averaged over the filament cross-section reduces to a diagonal, uniaxial form. Thus the normal stress

difference, $\Delta p = p_{zz} - p_{rr}$, can be expressed through axial tension, $F(z)$

$$\begin{aligned} &\mathbf{p} + \mathbf{I}\, p_0 = 2\eta\,(z)\,\dot{\mathbf{e}} = \eta\ \cdot\ \left(\nabla\mathbf{V} + \nabla\mathbf{V}^T\right), \\ &p_{zz} - p_{rr} = \Delta p = \frac{F(z)}{\pi R^2(z)} = 3\eta(z)\frac{dV}{dz}. \end{aligned} \tag{4.6}$$

With the above rheological behaviour, axial velocity gradient is obtained in the form

$$\frac{dV}{dz} = \frac{\rho V\left[F_0 + W(V - V_0)\right]}{3W\eta(z)}. \tag{4.7}$$

The apparent shear viscosity, $\eta$, is a function of position-dependent temperature, $T$, and local filament structure, characterized by the *degree of crystallinity* (volume fraction of crystalline phase) $X$:

$$\eta(z) = \eta\left[T(z), X(z)\right]. \tag{4.8}$$

The fact that rheological properties of the filament depend on crystallinity, $X$, introduces the necessity of considering the rate at which the structure is developed. The system of governing equations has to be completed with a *structure evolution equation.* Crystallization equation is assumed in the form of a non-isothermal, quasi-static Kolmogoroff–Avrami–Evans equation [6, 7]

$$\begin{aligned} &\frac{d\ln(1-X)}{dz} = -\frac{dE}{dz}, \\ &E = \left[\int_0^z \frac{K(z)}{V}\,dz\right]^n, \\ &\frac{dE}{dz} = n\left[\int_0^z \frac{K(z)}{V}\,dz\right]^{n-1}\frac{K(z)}{V}, \\ &\frac{d\ln(1-X)}{dz} = -nE^{(n-1)/n}\frac{K[T(z), \Delta p(z)]}{V}. \end{aligned} \tag{4.9}$$

Crystallization rate characteristic $K$ is controlled by local temperature, $T(z)$ and local normal stress difference $\Delta p(z)$.

## 5. Boundary conditions

The problem involves four first-order differential equations, respectively, for $V(z)$, $F(z)$, $T(z)$, and $X(z)$ and algebraic equation for radius $R(z)$, Eq. (4.1).

The conditions at the extrusion point, $z = 0$ read

$$\begin{aligned} R(z=0) &= R_0, \\ V(z=0) &= V_0, \\ F(z=0) &= F_0, \\ T(z=0) &= T_0, \\ X(z=0) &= 0. \end{aligned} \tag{5.1}$$

The initial tension, $F_0$, however, is not defined *a priori*. On the other hand, the process of spinning imposes another constraint on velocity at $z = L$. To obtain the take-up velocity $\mathrm{V}_L$ as a function of tension $F_0$, an *inverse problem* is solved. The values of $F_0$ are *assumed* and the corresponding take-up velocities, $V_L$, are calculated. The set of boundary conditions reduces to

$$\begin{aligned} R(z=0) &= R_0, \\ V(z=0) &= V_0, \\ V(z=L) &= V_L \quad \Leftrightarrow \quad F_0, \\ T(z=0) &= T_0, \\ X(z=0) &= 0. \end{aligned} \tag{5.2}$$

This is where the bifurcation appears: in some conditions the take-up velocity $V_L$ as a function of tension $F_0$ passes through a maximum (Figs. 2, 3).

## 6. Velocity profile and the criterion of bifurcation

Integration of Eq. (4.7) with boundary conditions (5.2) yields the axial velocity profile $V(z)$

$$\ln \frac{F_0 V(z)}{[F_0 + W(V - V_0)]\, V_0} = \frac{\rho\,(F_0 - WV_0)}{3W} \int_0^z \frac{dz}{\eta(z)} \tag{6.1}$$

and, at the end of the filament ($z = L$),

$$\ln \frac{F_0 V_L}{[F_0 + W(V_L - V_0)]\, V_0} = \frac{\rho\,(F_0 - WV_0)}{3W} \int_0^L \frac{dz}{\eta(z)} = \frac{\rho\,(F_0 - WV_0)}{3W} \cdot I_L\,(F_0, V_L)\,, \tag{6.2}$$

where $I_L$ is a functional describing effective fluidity (deformability) of the spinning line. Eq. (6.2) presents relationship between the two alternative boundary conditions $V(z=L)=V_L$ and $F(z=0)=F_0$.

Bifurcation appears when the take-up velocity, $V_L$, plotted vs. initial tension, $F_0$, is *maximum*. Putting

$$\frac{dV_L}{dF_0}=0 \tag{6.3}$$

we obtain the condition of bifurcation in the form

$$\left.\frac{\partial \ln I_L}{\partial \ln F_0}\right|_{\text{bifur}} = \frac{W\,(V_L-V_0)}{[F_0+W\,(V_L-V_0)]\ln\dfrac{F_0V_L}{V_0\,[F_0+W\,(V_L-V_0)]}} - \frac{F_0}{(F_0-WV_0)} \tag{6.4}$$

or:

$$\left.\frac{\partial \ln I_L}{\partial \ln F_0}\right|_{\text{bifur}} = \frac{\xi\,(S-1)}{[1+\xi\,(S-1)]\ln\dfrac{S}{1+\xi\,(S-1)}} - \frac{1}{(1-\xi)}$$

where $S=V_L/V_0$ is total elongation of the filament and $\xi=WV_0/F_0$ is the ratio of inertial force to viscous tension. Asymptotically

$$\begin{aligned} \xi\to 0: &\quad \left.\frac{\partial \ln I_L}{\partial \ln F_0}\right|_{\text{bifur}} = -1, \\ \xi\to \infty: &\quad \left.\frac{\partial \ln I_L}{\partial \ln F_0}\right|_{\text{bifur}} = 0. \end{aligned} \tag{6.5}$$

The necessary condition of bifurcation is *reduction of the fluidity integral* $I_L$ with increasing tension $F_0$, or *tension-induced solidification*. For slow, inertialess deformation ($\xi=0$) $I_L$ must be inversely proportional to $F_0$. It can be shown that the critical derivative $[\partial \ln I_L/\partial \ln F_0]_{\text{bifur}}$ monotonically increases with total deformation, $S$, and inertia, $\xi$, from $-1$ to zero. In real spinning conditions the inertia ratio is rather small ($\xi<1$) and the condition of bifurcation is confined to the range $(-0.5,\,-1.0)$.

## 7. Physical sources of tension-dependent fluidity

Reduction of the fluidity integral, $I_L$, with tension, $F_0$, results from variable shear viscosity. For the sake of simplicity we will present $\eta$ as a product of temperature-dependent and crystallinity-dependent functions

$$\eta(T,X)=\eta_T(T)\,\eta_X(X). \tag{7.1}$$

The expected variation of the integral $I_L$ may thus be controlled by the effects of temperature and/or crystallinity

$$I_L \equiv \int_0^L \frac{dz}{\eta_T\,[T(z)]\ \cdot \eta_X\ [X(z)]}\,,$$

$$\frac{\partial \ln I_L}{\partial \ln F_0} = -\frac{F_0}{I_L}\int_0^L \frac{1}{\eta}\left[\frac{\partial \ln \eta_T}{\partial T}\frac{\partial T}{\partial F_0} + \frac{\partial \ln \eta_X}{\partial X}\frac{\partial X}{\partial F_0}\right] dz \tag{7.2}$$

$$= \left.\frac{\partial \ln I_L}{\partial \ln F_0}\right|_{\text{temp}} + \left.\frac{\partial \ln I_L}{\partial \ln F_0}\right|_{\text{stress}}.$$

Before investigating various effects we will note that our early simulations which revealed bifurcation [1–3] were concerned with a specific material, linear polyethylene terephthalate. Standard material characteristics chosen from available data are listed in Table 1. In the course of analysing individual effects some of the standard characteristics were varied.

**Table 1. Standard material characteristics used.**

| Parameter | Equation No. | Standard value | Alternative values studied |
|---|---|---|---|
| Extrusion temperature, $T_0$, K | | 557 | |
| Maximum thermal crystallization rate temperature, $T_{\max}$, $K$ | (7.6) | 463 | |
| Melting temperature, $T_m$, K | (7.6) | 553 | |
| Glass-transition temperature, $T_g$, K | (7.6) | 340 | |
| Maximum thermal crystallization rate, $K_0$, $s^{-1}$ | (7.6) | $1.6 \times 10^{-2}$ | $1.6 \times 10^{1}$, $1.6 \times 10^{4}$ |
| Half-width of crystallization rate, $D$, K | (7.6) | 32 | |
| Stress-induced crystallization parameter, $A$ | (7.6) | 500 | 100, 50, 10, 5, 1, 0 |
| Activation energy for viscous flow, $E/k$, K | (7.4) | 6923.7 | 13847.4, 20771.1 |
| Viscosity-temperature function, $\eta_T(T;E)$ | (7.4) | Arrhenius | |
| Viscosity-crystallinity function, $\eta_X(X;X_{\text{crit}})$ | (7.5) | hyperbolic, $X_{\text{crit}} = 0.1$, $\alpha = 1$ | |

### 7.1. Effects of temperature-controlled viscosity

Polymer viscosity is a decreasing function of temperature, $T$. In the absence of crystallization reduction of the integral $I_L$ with increasing tension $F_0$, re-

quires such a change in the dynamics of the process that in the average, *local temperature is reduced* by tension $F_0$.

$$\eta_X = 1, \qquad \frac{\partial I_L}{\partial F_0} < 0 \;\Rightarrow\; \int_0^L \frac{1}{\eta}\left[\frac{\partial \ln \eta_T}{\partial T}\frac{\partial T}{\partial F_0}\right] dz \;>\; 0. \tag{7.3}$$

Viscosity of polymer melts can be described with the simple Arrhenius model

$$\eta_T(T) = \eta_0 e^{E/kT}, \tag{7.4}$$

where $E$ is activation energy. The higher is $E$, the more steep will be the increase of viscosity with reciprocal temperature. To analyse the effects of $\eta_T$ on bifurcation we will compare three functions with different parameters $E$ and $\eta_0$. The functions are normalized to produce the same viscosity at the extrusion temperature $T_0 = 573$ K (Table 2).

**Table 2. Parameters of the Arrhenius viscosity-temperature function.**

| Activation energy, $E/k$, K | $\eta_0$ Pas | $\eta$(573 K), Pas extrusion | $\eta$(340 K), Pas glass transition |
|---|---|---|---|
| 6923.7 | $6.547 \times 10^{-4}$ | $1.158 \times 10^{2}$ | $4.570 \times 10^{5}$ |
| 13847.4 | $3.701 \times 10^{-9}$ | $1.158 \times 10^{2}$ | $1.803 \times 10^{9}$ |
| 20771.1 | $2.092 \times 10^{-14}$ | $1.158 \times 10^{2}$ | $7.116 \times 10^{12}$ |

Figure 4 presents $V_L$ vs. $F_0$ plots for three viscosity-temperature functions controlled by different activation energies. It is evident that in the range studied, no bifurcation was observed.

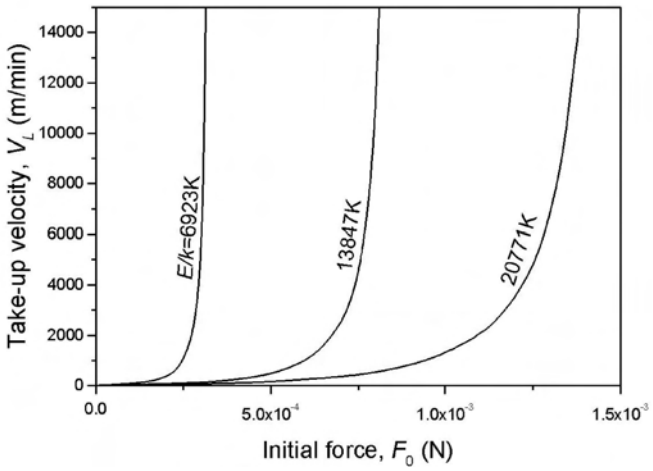


FIG. 4. Velocity-tension relations for polymer melts with temperature-controlled viscosity ($\eta_X = 1$). Reduced activation energies, $E/k$, indicated.

### 7.2. Effects of crystallization

**7.2.1. Viscosity vs. crystallinity.** Rheological properties of polymer melts are known to be sensitive to crystallization. In contrast to rigid-particle suspensions, small amounts of crystalline phase can make viscosity of polymer melts higher by some orders of magnitude, ultimately converting viscous fluid into a plastic solid [8–10]. This effect is often visualised [8, 10, 11] as *crosslinking* of linear polymer chains. Small crystals (nuclei?) bind polymer chains together acting as *physical crosslinks*. When the number of such interchain bonds reaches the critical level (approximately two bonds per primary chain), a solid rubberlike *network* is obtained.

In the course of crystallization, the polymer melt consisting of entangled chains is gradually converted into a system of aggregates and, when density of crystals reaches the critical level, $X_{\mathrm{crit}}$, into a rubberlike network (Fig. 5).

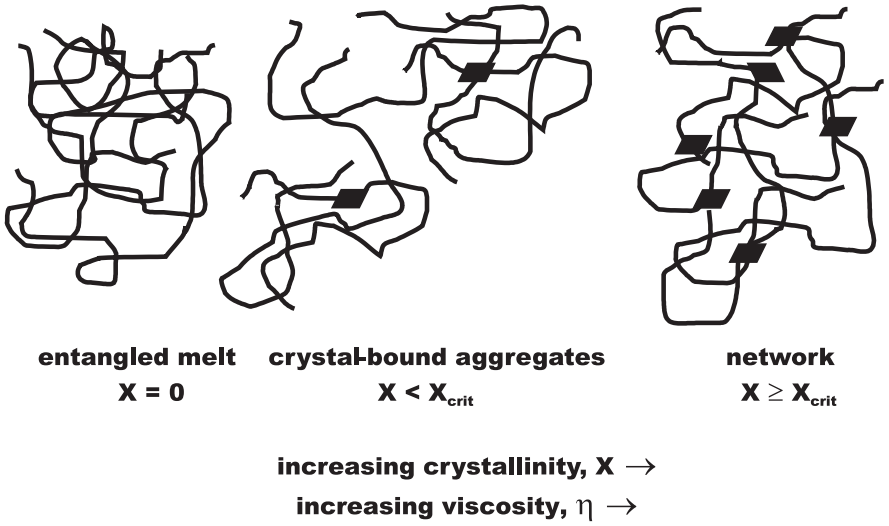


Fig. 5. Model of crystallization-affected viscosity of polymer melt.

Simple model describing such a behaviour has been proposed in Ref. [11]

$$\eta_X = \begin{cases} 1 & X = 0, \\ \left[\dfrac{X_{\mathrm{crit}}}{X_{\mathrm{crit}} - X}\right]^{\alpha} & X < X_{\mathrm{crit}}, \\ \infty & X \geq X_{\mathrm{crit}}. \end{cases} \tag{7.5}$$

Hyperbolic function Eq. (7.5) predicting abrupt viscosity increase near $X = X_{\text{crit}}$ was used in our earlier simulations for PET [1–4]. Similar function was used by KRIEGER and DOUGHERTY [12] for viscosity of concentrated suspensions.

**7.2.2. Crystallization rates.** Crystallization of long-chain polymers is very sensitive to temperature and stress. Moderate stresses elevate the crystallization temperature and crystallization rates. The latter may increase by several orders of magnitude compared to unstressed systems [13, 14].

The crystallization rate function $K$ in Eq. (4.9) is considered in the form [15]

$$K[T, \Delta p] = K_T(T) \cdot K_{\text{stress}}(\Delta p),$$

$$K_T(T) = \begin{cases} K_0 e^{-4 \ln 2 (T - T_{\max})^2 / D^2} & \text{for} \quad T_g < T < T_m, \\ 0 & \text{for} \quad T \le T_g \quad \text{or} \quad T \ge T_m, \end{cases} \tag{7.6}$$

$$K_{\text{stress}}(\Delta p) = \exp\left[ A \left( \frac{\Delta p}{\Delta p_i} \right)^2 \right].$$

The temperature-controlled part $K_T(T)$, is assumed in the form of a Gaussian function with maximum value $K_0$ at $T = T_{\max}$ and half-width $D$. The function is truncated on both ends of the crystallization interval. The lower temperature limit is determined by vanishing translational mobility at the glass transition temperature, $T_g$; above the upper limit (melting temperature, $T_m$) crystallization is excluded thermodynamically. The exponential form of the stress-controlled function $K_{\text{stress}}$ was found useful in interpretation of experimental data [14]. $\Delta p_i$ denotes the stress level required for practically complete extension of polymer chains.

Variation of crystallization rate in the evolution equations (4.9) and, consequently, the degree of crystallinity, $X$, and viscosity, $\eta$, with tension $F_0$, is

$$K(T, \Delta p) = K_T(T) \cdot K_{\text{stress}}(\Delta p),$$

$$\frac{\partial K}{\partial F_0} = K(T, \Delta p) \left[ \frac{\partial \ln K_T}{\partial T} \frac{\partial T}{\partial F_0} + \frac{\partial \ln K_f}{\partial f} \frac{\partial f}{\partial F_0} \right] = \left. \frac{\partial K}{\partial F_0} \right|_{\text{therm}} + \left. \frac{\partial K}{\partial F_0} \right|_{\text{stress}} \tag{7.7}$$

and includes thermal and stress effects.

**7.2.3. Thermal crystallization.** Consider the crystallization rate controlled by temperature only. Using the model equations (7.5), the dependence of thermal crystallization rate on tension is obtained in the form

$$K_{\text{stress}}(\Delta p) = 1,$$

$$\left.\frac{\partial K}{\partial F_0}\right|_{\text{therm}} = \frac{\partial K_T}{\partial T}\frac{\partial T}{\partial F_0} = \frac{-8\ln 2(T - T_{\max})}{D^2} K_0 e^{-4\ln 2(T-T_{\max})^2/D^2}\frac{\partial T}{\partial F_0}. \tag{7.8}$$

Thermal crystallization rate passes through a maximum and the sign of $\partial T/\partial F_0$ can be different at different positions $z$ in the melt. To analyse the effect of thermal crystallization on bifurcation, we have plotted $V_L$ vs. $F_0$ functions for three different $K_0$ values. The Gaussian-type thermal crystallization rate function (Eq. (7.7)) was combined with hyperbolic viscosity-crystallinity function (Eq. (7.6)). The results presented in Fig. 6 show that in the absence of stress-induced crystallization, the take-up velocity $V_L$ monotonically increases with tension $F_0$.

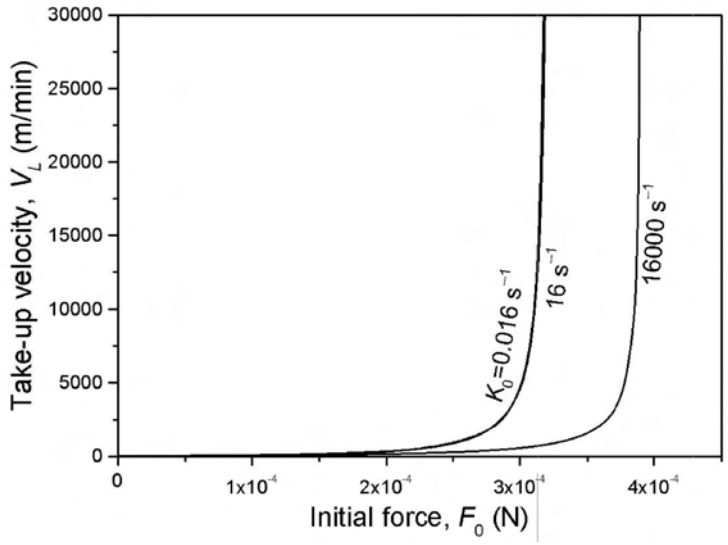


FIG. 6. Velocity-tension relations for crystallizing polymer melts. Standard hyperbolic viscosity-crystallinity function, $\eta_X$, is combined with thermal crystallization. Crystallization rates, $K_0$ indicated.

With increasing crystallization rate, $K_0$, the upturn of the velocity-tension functions is shifted to higher tensions, $F_0$, but their monotonic shape is unchanged.

**7.2.4. Stress-induced crystallization.** Last but not least, we will discuss polymer crystallization induced by stress. Crystallization rate controlled by stress reads

$$\left.\frac{\partial K}{\partial F_0}\right|_{\text{stress}} = K_T(T)\frac{\partial K_{\text{stress}}}{\partial \Delta p}\frac{\partial \Delta p}{\partial F_0} = \frac{2A\Delta p}{(\Delta p_i)^2}K_T(T)\, e^{A\left(\frac{\Delta p}{\Delta p_i}\right)^2}\frac{\partial \Delta p}{\partial F_0},$$

$$\Delta p = \frac{\rho V[F_0 + W(V - V_0)]}{W}, \tag{7.9}$$

$$\frac{\partial \Delta p}{\partial F_0} = \frac{\Delta p}{F_0 + W(V - V_0)}\left[1 + (F_0 + W(2V - V_0))\frac{\partial \ln V}{\partial F_0}\right].$$

Now tension, $F_0$, and normal stress, $\Delta p$, appear explicitly in the expressions for crystallization rate and obviously will contribute to crystallinity, $X$. Figures 7–9 present $V_L$ vs. $F_0$ plots at three different thermal crystallization rates combined with different stress-induced crystallization coefficients, $A$. The calculations have been performed using standard Arrhenius viscosity and standard hyperbolic viscosity-crystallinity relation (Table 1).

At small and medium values of $K_0$, bifurcation is evidently starting with some critical $A$.

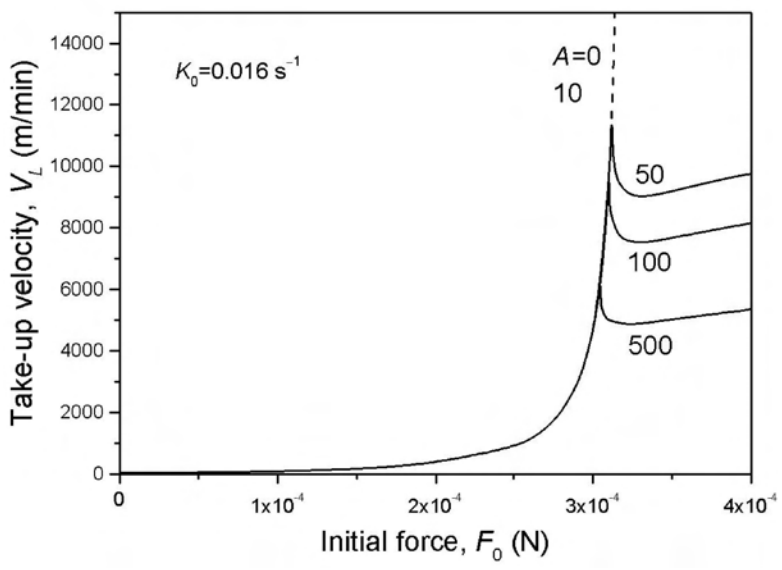


FIG. 7. Velocity-tension relations for crystallizing melts. Standard hyperbolic viscosity-crystallinity function combined with stress-induced crystallization. Thermal crystallization rate, $K_0 = 0.016\ \text{s}^{-1}$, stress-induced crystallization rate coefficients, $A$, indicated.

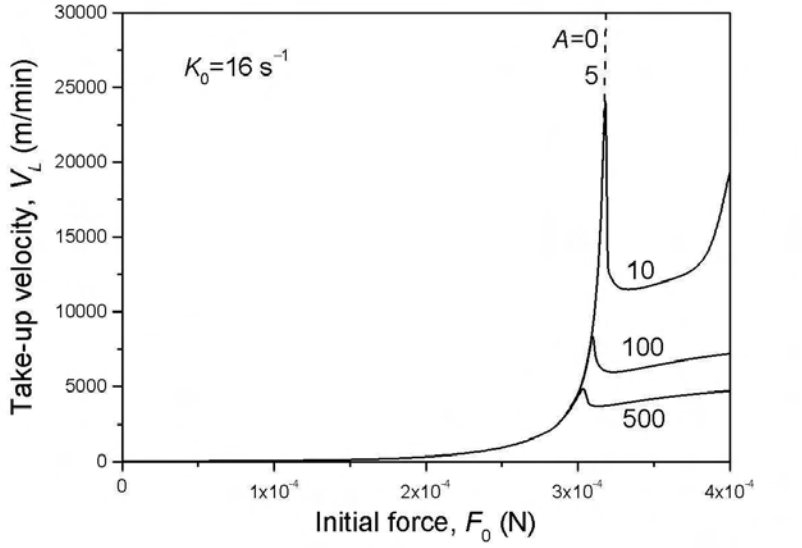


Fig. 8. Velocity-tension relations for crystallizing melts. Standard hyperbolic viscosity-crystallinity function combined with stress-induced crystallization. Thermal crystallization rate, $K_0 = 16000$ s$^{-1}$, stress-induced crystallization rate coefficients, A, indicated.

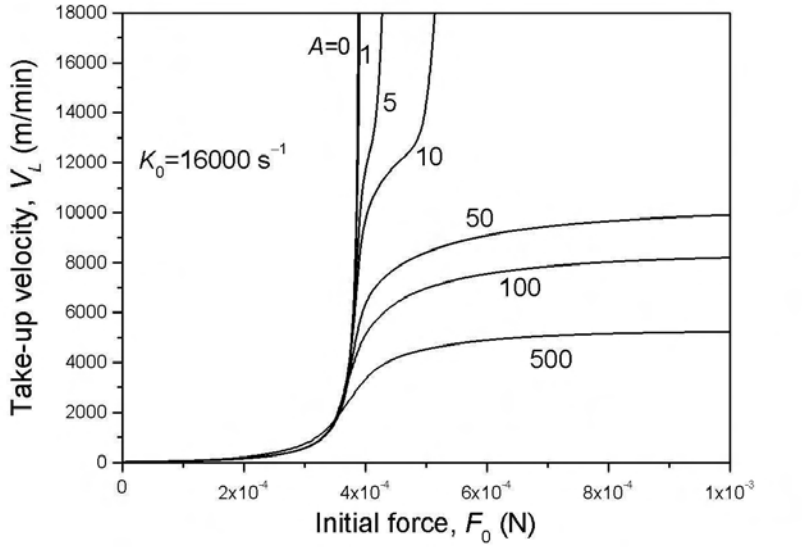


Fig. 9. Velocity-tension relations for crystallizing melts. Standard hyperbolic viscosity-crystallinity function combined with stress-induced crystallization. Thermal crystallization rate, $K_0 = 16$ s$^{-1}$, stress-induced crystallization rate coefficients, $A$, indicated.

Different behaviour is observed when thermal crystallization rate is very high (Fig. 9). At $K_0 = 1600\ \mathrm{s}^{-1}$ the $V_L - F_0$ plots are monotonically increasing. At $A = 0$ the plot is concave, at small $A = 1 - 10$ it is $S$-shaped with two inflexion points, and at high $A = 50 - 500$ it is $S$-shaped with one inflexion point.

The behaviour at high crystallization rates (both thermal and stress-induced) seems to result from rapid solidification requiring higher and higher tensions for flow deformation. It is interesting to note that $S$-shaped $V_L - F_0$ characteristics restrict admissible spinning conditions (maximum), although no bifurcation appears.

## 8. Discussion

We have demonstrated that in some conditions, solutions of the dynamic equations of melt spinning show *bifurcation.* Bifurcation results from stress-controlled solidification of the fluid polymer. Temperature effects seem to be of secondary, if any, importance. The decisive role is played by crystallinity-controlled viscosity combined with stress-induced crystallization. In some regimes (moderate thermal crystallization rates, strong stress-induced crystallization effects) maximum take-up velocity cannot be surpassed. In other regimes (high thermal and stress-induced crystallization rates), small increase of spinning velocity requires extremely high tensions and may result in fracture of the solidifying polymer jet.

It is interesting to note that other authors who studied dynamics of melt spinning in crystallizing polymers [16–19] did not report bifurcation. The reasons may be different polymers and different material characteristics considered. Our model was designed primarily for polyethylene terephthalate known to crystallize very slowly in the absence of stress (low $K_0$) and change the crystallization rates by many orders of magnitude under small and moderate stress. These are typical requirements for the bifurcation shown in Figs. 2, 3, 7, and 8. On the other hand, behaviour of polymers crystallizing rapidly without stress (high $K_0$), like polyethylene or polyamides, may correspond to the pattern presented in Fig. 9.

The nature of the bifurcation phenomenon deserves some reflection. Bifurcation in strictly steady conditions does not necessarily imply instability. In some range of spinning conditions the system of nonlinear equations has two stable solutions. It is difficult to say which of the two solutions is physically more justified. One might be inclined to choose the solution with lower energy. Perturbation of spinning conditions and/or material properties may induce instability consisting in jumping from one solution to the other one. An important consequence of bifurcation is limitation of the accessible spinning conditions. In absence of the crystallization-induced bifurcation, non-isothermal spinning

of a Newtonian polymer can be performed in any conditions (up to cohesive fracture of the material).

In contrast to isothermal spinning exhibiting draw-resonance instability, non-isothermal spinning of a Newtonian fluid is inherently stable [20, 21]. The Newtonian model is oversimplified and introduction of viscoelasticity may induce instability in the conditions where bifurcation of steady solutions does not appear. The onset of viscoelastic instability is controlled by critical value of deformation rate and relaxation time combined into the dimensionless product, *the Deborah number* e.g. [21, 22].

Practical significance of the observed phenomenon consists in *limitation* of the *accessible spinning conditions*. Experimental observations on melt spinning of PET fibres are qualitatively consistent with predictions following from the bifurcation analysis. Maximum take-up velocity increases with increasing filament thickness and reduced by increasing polymer viscosity. In a recent PhD Thesis in our laboratory [23], the calculated maximum take-up velocity for spinning 5 dtex PET filaments vs. molecular weight $M_\eta$ in the range of 20000–40000 were compared with experimental data [24]. The results showing three regions: low-speed-spun spinning of amorphous fibres, intermediate-speed-spun crystalline fibres and supercritical speeds inaccessible to spinning, were reasonably consistent with Huisman *et al.* observations.

In a recent paper [25] instability of viscoelastic spinning of isotactic polypropylene was studied. It was found that the onset of instability leads to limitation of accessible spinning conditions in a way similar to that caused by bifurcation. The inaccessible range of spinning conditions was predicted with, or without crystallization. However, introduction of flow-induced crystallization considerably enhanced the inaccessible range.

## References

1. L. Jarecki, A. Ziabicki, A. Blim, *Dynamics of hot-tube spinning from crystallizing polymer melts*, Comput. Theoret. Polymer Sci., **10**, 63–72, 2000.
2. L. Jarecki, A. Ziabicki, *Viscosity effects in computer modelling of fiber spinning from crystallizing polymer melts* [in English], Polimery, **49,** 101, 2004.
3. A. Blim, E. Ołdak, A. Wasiak, L. Jarecki, *Effect of zone heating on the structure of PET fibers and the dynamics of melt spinning* [in Polish], Polimery, **50,** 48–59, 2005.
4. A. Ziabicki, L. Jarecki, A. Wasiak, *Dynamic modelling of melt spinning*, Comput. Theoret. Polymer Sci., **8**, 143–157, 1998.
5. S. Kase, T. Matsuo, *Studies on melt spinning. I. Fundamental equations on the dynamics of melt spinning*, J. Polymer Sci., **A3**, 2541, 1965; *II, Steady-state and transient solutions of fundamental equations compared with experimental results*, J. Appl. Polymer Sci., **11**, 251–287, 1968.

6. A. ZIABICKI, *Kinetics of polymer crystallization and molecular orientation in the course of melt spinning*, Appl. Polymer Symposia, **6** 1, 1967; *Crystallization of polymers in variable external conditions*, Colloid and Polymer Sci., **274**, 209, 1996.

7. K. NAKAMURA , T. WATANABE, K. KATAYAMA, T. AMANO, *Some aspects of non-isothermal crystallization of polymers, I. Relationship between crystallization temperature, crystallinity and cooling conditions*, J. Appl. Polymer Sci., **16**, 1077–1099, 1972; *II. Consideration of the isokinetic condition*, ibid, **17**, 1031–1041, 1973.

8. Y.G. LIN, D.T. MALLIN, J.C.W. CHIEN, H.H. WINTER, *Dynamic mechanical measurement of crystallization induced gelation in thermoplastic polypropylene*, Macromolecules, **24**, 850, 1991.

9. G. FLOUDAS, L. HILLIOU, D. LELLINGER, I. ALIG, *Shear-induced crystallization in poly-e-caprolactone,* Macromolecules, **30**, 6466, 2000.

10. C. SCHWITTAY, M. MOURS, H.H. WINTER, *Rheological expression of physical gelation in polymers*, Faraday Disc., **101**, 93–104, 1995.

11. A. ZIABICKI, *The mechanisms of neck-like deformation in high-speed melt spinning. 2. Effects of polymer crystallization*, J. Non-Newtonian Fluid Mech., **30**, 157–168, 1988.

12. I.M. KRIEGER, T.J. DOUGHERTY, *A mechanism for non-Newtonian flow in suspensions of rigid spheres*, Trans. Soc. Rheol., **3,** 137–152, 1959.

13. A. ZIABICKI, L. JARECKI, [in:] *High Speed Fiber Spinning*, A. ZIABICKI, H. KAWAI, [Eds.], Wiley, N.Y. p. 225, 1985.

14. G.C. ALFONSO, M.P. VERDONA, A. WASIAK, *Crystallization kinetics of oriented polyethylene terephthalate in the glassy state*, Polymer, **19**, 711–716, 1978.

15. A. ZIABICKI, [in:] *Fundamentals of Fiber Formation* Wiley, London, p. 113, 1976.

16. A. MAKRADI, S. AHZI, RV. GREGORY, *Effects of non-isothermal oriented crystallization on the velocity and elongational viscosity profiles during the melt spinning of HDPE fibers*, Polymer Engineering and Sci., **41**, 1107–1114, 2001.

17. A.K. DOUFAS, A.J. MCHUGH, C. MILLER, *Simulation of melt spinning including flow-induced crystallization. I. Model development and predictions,* J. Non-Newtonian Fluid Mech., **92**, 27, 2000; *II. Quantitative comparisons with industrial spinline data*, **92**, 81, 2000.

18. K. KANNAN, K.R. RAJAGOPAL, *Simulation of fiber spinning including flow-induced crystallization,* J. Rheol., **49**, 683, 2005.

19. J.A. KULKARNI, A.N. BERIS, *A model for the necking phenomenon in high-speed fiber spinning based on flow-induced crystalization*, J. Rheol., **42**, 971–994, 1998.

*Received September 20, 2005; revised version December 27, 2005.*